Simulation of the Part Load Behavior of Combined Heat Pump-Organic Rankine Cycle Systems

Bernd Eppinger [1,*], **Mustafa Muradi** [1], **Daniel Scharrer** [2], **Lars Zigan** [1], **Peter Bazan** [2], **Reinhard German** [2] **and Stefan Will** [1]

1 Institute of Engineering Thermodynamics (LTT), Friedrich-Alexander-Universität Erlangen-Nürnberg (FAU), 91058 Erlangen-Tennenlohe, Germany; mustafa.muradi@fau.de (M.M.); lars.zigan@fau.de (L.Z.); stefan.will@fau.de (S.W.)

2 Lab of Computer Networks and Communication Systems, Friedrich-Alexander-Universität Erlangen-Nürnberg (FAU), 91058 Erlangen, Germany; daniel.scharrer@fau.de (D.S.); peter.bazan@fau.de (P.B.); reinhard.german@fau.de (R.G.)

* Correspondence: bernd.eppinger@fau.de

Abstract: Pumped Thermal Energy Storages (PTES) are suitable for bridging temporary energy shortages, which may occur due to the utilization of renewable energy sources. A combined heat pump (HP)-Organic Rankine Cycle (ORC) system with suitable thermal storage offers a favorable way to store energy for small to medium sized applications. To address the aspect of flexibility, the part load behavior of a combined HP-ORC system, both having R1233zd(E) (Trans-1-chloro-3,3,3-trifluoropropene) as working fluid and being connected through a water filled sensible thermal energy storage, is investigated using a MATLAB code with integration of the fluid database REFPROP. The influence on the isentropic efficiency of the working machines and therefore the power to power efficiency (P2P) of the complete system is shown by variation of the mass flow and a temperature drop in the thermal storage. Further machine-specific parameters such as volumetric efficiency and internal leakage efficiency are also considered. The results show the performance characteristics of the PTES as a function of the load. While the drop in storage temperature has only slight effects on the P2P efficiency, the reduction in mass flow contributes to the biggest decrease in the efficiency. Furthermore, a simulation for dynamic load analysis of a small energy grid in a settlement is conducted to show the course of energy demand, supplied energy by photovoltaic (PV) systems, as well as the PTES performance indicators throughout an entire year. It is shown that the use of PTES is particularly useful in the period between winter and summer time, when demand and supplied photovoltaic energy are approximately equal.

Keywords: thermal energy storage; fluid mass flow; temperature; part load; simulation; Carnot battery

1. Introduction

Pumped Thermal Energy Storages (PTES) cover only a small part of the entire spectrum of energy storage systems [1]. They consist of a theoretically reversible thermodynamic cycle for charging and discharging a thermal energy storage [2,3]. The storage itself can be further subdivided into latent [4–6], sensible [7–9], and thermochemical energy storages [10], of which only the sensible thermal water storage [11] is considered in this paper. Generally, energy storage is used to compensate for discrepancies between required and supplied energy, which occur more frequently when the energy system relies on renewable energy sources. The flexibility of the PTES mainly depends on its part load behavior, which can be analyzed in a model via a change in mass flow for the heat pump (HP) and Organic Rankine Cycle (ORC) operations, as well as a temperature drop in the sensible thermal storage. In Martinot's [12] work, the aspect of flexibility was treated from both the supply and the demand sides, suggesting that both parts can contribute to an adapted relationship

between energy production and consumption. An investigation of the part load behavior of PTES helps in our understanding of the aspect of integration of energy storage systems in flexible energy grids, which rely on renewable energies to a higher degree [13,14].

There are various scientific studies that deal specifically with the combination of an HP as well as an ORC but with different foci. The selection of fluids is examined more closely for a performance evaluation in the recent work of Wu et al. [15], whereas Lecompte et al. [16] and Mounier et al. [17] carried out thermo-economic optimizations. While Koohi-Fayegh and Rosen [18] give a rough overview of energy storage types, applications, and recent developments, the work of Delgado et al. [19] focused on modifying the thermal storage technology to compensate for the fluctuations of renewable energy. This was done using a computational fluid dynamics (CFD) simulation. Additionally, a simplified demand assessment model was adopted. The results are promising, as savings of over 40% in heat demand are possible. Lee at al. [20] investigated the part load ratio characteristics of a ground source heat pump (GSHP) connected to a storage, suggesting that energy savings of 10.1% for cooling and 20.8% for heating could be achieved, compared to the case without a storage. Anderson and Morrison [21] determined the performance of a solar-boosted heat pump water heater (HPWH) operating under full load and part load conditions in an outdoor experimental study, observing the COP at different times of the day. On the other hand, core research on ORC performance analysis has been done. For example, Wang et al. [22] conducted a general performance study for four different kinds of ORC and studied the effects of thermodynamic conditions on performance, Ziviani et al. [23] conduced a performance analysis on working machines such as a single-screw and scroll expander, concluding that the single-screw expander has a higher power output and leads to a higher overall ORC efficiency. However, scroll expanders have the potential to be suitable for domestic-scale ORC systems, since there is no notable difference in the ORC efficiency when considering a low power output range.

In the present paper, low temperature waste heat is utilized to bring an organic working fluid to a higher temperature level by applying a heat pump powered by excess energy from PV systems. The hot fluid then charges the water filled sensible thermal storage, which powers the ORC during energy demand. Since it is a combined system, components like the heat exchangers and the working fluid are used in both operation modes. Moreover, the working machine is operated as a compressor for the heat pump process as well as an expander in the ORC-mode. In this work, the thermal storage temperature ranged from 90 °C to 120 °C. Trans-1-chloro-3,3,3-trifluoropropene (R1233zd(E)) was used, among others, as a working medium in Eppinger et al. 2020 [24]. Its physical properties were found to be favorable for increasing efficiency. In the present paper, for a closer look at the performance characteristics, the heat pump's coefficient of performance (COP) and ORC efficiency are displayed as a function of the load, which can be set by varying the mass flow as well as a temperature drop in the thermal storage. In this frame, the storage temperature may vary due to extensive storage time. To put those parameters into context, the power-to-power (P2P) efficiency is examined in more detail. Furthermore, the annual development of various system parameters and performance indicators is presented for a small existing energy grid of a settlement equipped with PV and PTES. There are no studies known to the authors that performed simulations on a similar topic regarding PTES or used any real-world data to show integration with a certain power grid. With rising shares of renewable energies in certain energy grids, it is important to understand the effects of the part load behavior of flexible energy storage, which is the focus of this paper.

2. Materials and Methods

Based on the previous research of Eppinger et al. conducted in 2019 [25] and in 2020 [24], the modeled setup of the PTES consists of a heat pump and an ORC, which are connected through a sensible thermal storage. The same MATLAB code with integration of the fluid data from REFPROP was applied here. However, in this paper the focus is put on the part load behavior of PTES in general and in a certain energy grid. The basic code

has been validated by code-to-code verification with a model in Dymola, see reference Eppinger et al. 2020 [11] for more details.

2.1. Heat Pump

In this research, a screw compressor was chosen as a working machine for the present simulation. This selection is based on the work of Liu et al. [26], who explained the effects of certain parameters on variables such as the isentropic efficiency in detail. This was done by building a screw compressor model on the basis of experimental data regression. It was concluded that the model is precise enough for simulation of a refrigeration system. A broader description of screw compressor performances in terms of their application range was given by Wennemar [27] revealing a variety of dependencies of different parameters. Different effects were studied, such as the rotor diameter or the molecular weight of the working fluid on the adiabatic efficiency and the associated power output. In the present study, the same working machine is used as an expander in the ORC. In general, other types of compressors could have been used instead. For example, a scroll compressor was used for the heat pump compressor as well as for the ORC expander in the work of Dumont et al. [28].

In general, the coefficient of performance (COP) of the HP is defined as

$$COP_{HP} = \frac{-\dot{Q}_{HP,out}}{P_{HP,comp.,el.}} \tag{1}$$

describing the ratio between the usable heat $\dot{Q}_{HP,out}$, which is at a higher temperature level compared to the environment, and the power $P_{HP,comp.,el.}$ required by the compressor.

2.2. ORC

Since the system operates in a low temperature range, an ORC is used to generate electrical energy. Detailed descriptions of an ORC can be found in Yamamoto et al. [29]. The ORC represents the reciprocal process of the heat pump using the same working fluid.

To assess the influence of the part load on the ORC, the ORC efficiency η_{ORC} was examined more closely, which is defined as

$$\eta_{ORC} = \frac{-P_{ORC,el.}}{\dot{Q}_{ORC,in}}. \tag{2}$$

It represents the ratio between the utilized electrical power $P_{ORC,el.}$ obtained from the ORC and the heat flow $\dot{Q}_{ORC,in}$ absorbed by the thermal storage.

2.3. Combined System

Heat pump and ORC are connected through a sensible thermal energy storage. Figure 1 shows a schematic thermodynamic cycle of both processes including their state points T, s-diagram, as well as the charging and discharging of the thermal storage with its temperature profile. Further details are given in reference [24].
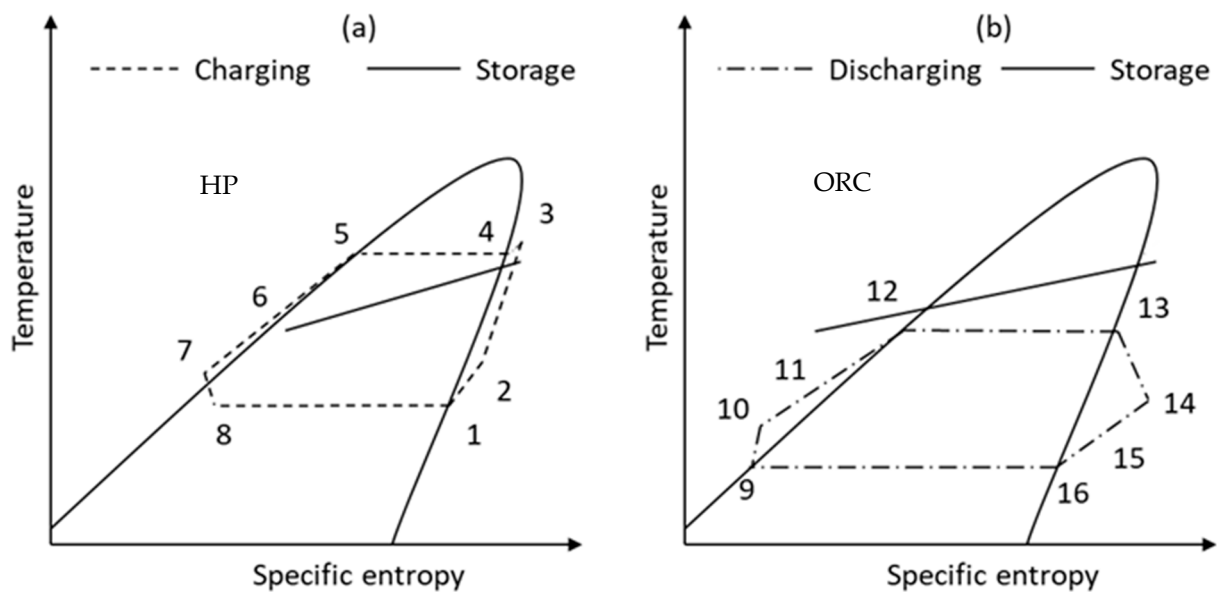
Figure 1. Schematic cycles of the heat pump (a) and ORC (b) in the *T, s*-diagram including the temperature profile of the sensible thermal storage (solid lines) [24].

1–2 superheating with internal heat exchanger (HX)	9–10 pressure change via feed pump
2–3 compression of superheated vapor	10–11 preheating in the internal HX
3–4 desuperheating in the thermal storage HX	11–12 preheating in the thermal storage HX
4–5 condensation in the thermal storage HX	12–13 evaporation in the thermal storage HX
5–6 sub-cooling in the thermal storage HX	13–14 expansion in the working machine
6–7 sub-cooling in the internal HX	14–15 desuperheating in the internal HX
7–8 isenthalpic expansion via throttle	15–16 desuperheating in the condenser
8–1 evaporation in the waste HX	16–9 condensation in the condenser

The P2P efficiency represents the link between the heat pump and the ORC for the whole PTES. It is obtained through the product of the COP, the ORC efficiency η_{ORC} and the efficiency of the thermal energy storage η_{st}. However, according to the reference case, shown in Section 2.5, the latter is set to 100%. The equation reads as follows:

$$P2P = COP_{HP} \cdot \eta_{ORC} \cdot \eta_{st}. \tag{3}$$

2.4. Definition of the Part Load Behavior

For a closer look into the part load operation, its influence on the mass flow as well as the temperature drop in the thermal storage is examined more closely. In addition, the isentropic efficiency is adjusted to the part load conditions. On the one hand, the part load defined by the mass flow of the HP is a result of the available power, while for the ORC it is a result of the demand curve, respectively, and is therefore actively controlled. On the other hand, the part load of the system defined by the temperature drop in the thermal storage is not controllable, but it is a result of the loss of thermal energy from the storage.

2.4.1. Realization of Part Load via Altered Mass Flow

Reducing the mass flow rate is a variant for realizing part load operation:

$$\dot{m}_{PL} = \dot{m}_{FL} \cdot \alpha \tag{4}$$

The part load mass flow $\dot{m}_{PL}$ is obtainable in our model by multiplying the mass flow at full load conditions $\dot{m}_{FL}$ with the load α, which can be set from 0% to 100%. Additionally, there is a direct correlation between mass flow and heat flow via the enthalpy:

$$\dot{Q} = \dot{m} \cdot \Delta h \tag{5}$$

The mass flow influences the selection of working machines (HP compressor as well as the ORC expander) and their respective efficiencies:

$$\eta_{HP,comp./ORC,exp.,PL} = \eta_{HP,comp./ORC,exp.,FL} \cdot \eta_m \qquad (6)$$

The HP compressor efficiency or the ORC expander efficiency are additionally multiplied by the motor efficiency η_m, which depends on the set load α. The motor efficiency was taken from Liu et al. [26] and can be considered representative, since their work showed that the modeled system did not differ much from the one in the field test. More importantly, the framework was similar to that of the present paper.

The progression of η_m is provided in Figure 2.
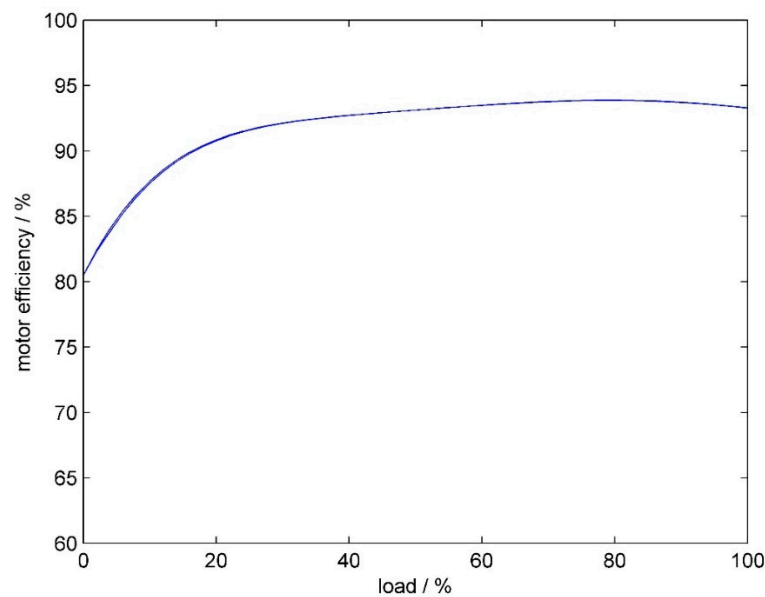

Figure 2. Curve of motor efficiency as a function of the load according to Liu et al. [26].

2.4.2. Realization of Part Load via the Temperature Drop of the Thermal Energy Storage

Having a drop in the upper temperature of the thermal energy storage, which occurs due to extensive storage time, will ultimately affect the pressure level of the ORC. In the relevant range, the change of the saturation pressure with temperature is about 19.2 kPa/K, which can be taken from the vapor pressure curve of R1233zd(E), which is attached in the Appendix A.

In general, the results of He et al. [30] showed that for screw expanders, a good working efficiency is obtained at higher pressure levels as well as at high rotational speeds. This means that the temperature drop leads to lower efficiency of screw expanders.

A temperature difference ΔT_{PL} was introduced to reduce the maximum storage temperature during part load (PL) operation:

$$T_{st,max,PL} = T_{st,max,FL} - \Delta T_{PL}. \qquad (7)$$

ΔT_{PL} is in the range of 0 K to 25 K in the present study, see Appendix A Figure A1 for the effect of the temperature drop on the pressure of the working fluid.

2.4.3. Adjustment of the Isentropic Efficiency

While Erhart et al. [31] discussed the isentropic efficiency's mass flow dependency, it is also affected by the drop of the storage temperature or by the change of the pressure ratio, respectively, which was outlined by Liu et al. [26].

In order to cover all influences in the isentropic part load efficiency $\eta_{s,\,PL}$, the full load (FL) isentropic efficiency $\eta_{s,standard}$ is multiplied by part load (PL) correction factors as follows:

$$\eta_{s,\,PL} = \eta_{s,standard} \cdot \frac{\eta_{v,PL} \cdot \eta_{n.PL}}{\eta_{v,FL} \cdot \eta_{n.FL}}. \tag{8}$$

For part load conditions, two parameters must be considered: The volumetric efficiency η_v represents the efficiency of the compressor cylinder and is dependent on the suction pressure and discharging pressure. The internal leakage efficiency η_n describes leakages occurring during compression. Those parameters are also dependent on the load. The volumetric efficiency can be described by the empirical and simplified relationship established by Liu et al. [26]:

$$\eta_v = 0.95 - 0.0125 \cdot \frac{p_2}{p_1}. \tag{9}$$

There is only a dependence on the pressure ratio in formula 9. Moreover, a linear progression of the volumetric efficiency has been proven in the research of Gonçalves et al. [32], which allows the use of linear interpolation to consider the volumetric efficiencies of other operating points.

The following applies to the internal leakage efficiency η_n:

$$\eta_{n,PL} = \eta_{n,FL} \cdot f(\alpha) \tag{10}$$

where $f(\alpha)$ is a correction function that depends on the mass flow or load α. It is obtained through the following equation, which is also taken from Liu et al. [26]:

$$f(\alpha) = 0.00294 \cdot \alpha + 0.706 \tag{11}$$

Since Liu et al. demonstrated a linear relationship between volumetric efficiency and internal leakage efficiency, the internal leakage efficiency for full load operation is accessible through linear regression:

$$\eta_{n,FL} = d \cdot \eta_{v,FL} + e \tag{12}$$

Here, d and e are regression coefficients representing the slope of the line and the y-axis intercept. They are calculated through interpolation between two values of η_v at different pressure ratios, which are obtained by simulation runs without considering part load influences. In this work, the regression coefficients are $d = 0.872$ and $e = 0.022$.

2.5. Reference Case

For a clearer and more uniform presentation of the results, reference conditions for the simulation are chosen, which refer to the working machines of the PTES, i.e., the HP (see Table 1), the sensitive thermal storage (see Table 2) and the ORC (see Table 3). The reference case is a direct result of the optimizations of the former studies presented by Eppinger et al. in 2020 [24] and the design goals of Eppinger et al. in 2021 [33]. Quantities of the high-pressure side of both cycles (condensation temperature in the HP process, sub-cooling temperature in the HP process) are initial values and are calculated during the simulation to fit the chosen pinch point temperatures in both cycles.

Table 1. Reference parameters of the heat pump.

Parameter	Abbreviation	Value	Unit
Evaporation temperature in the heat pump process	$t_{HP,in}$	75	°C
Superheating temperature in the heat pump process	$\Delta t_{HP,sh}$	0	°C
Condensation temperature in the heat pump process	$t_{HP,out}$	122	°C
Sub-cooling temperature in the heat pump process	$\Delta T_{HP,sc}$	30	K
Pressure loss during evaporation in the heat pump process	$\Delta p_{HP,evap.}$	0	bar
Pressure loss during condensation in the heat pump process	$\Delta p_{HP,cond.}$	0	bar
Isentropic efficiency of the heat pump process	$\eta_{s,HP}$	70	%
Electrical efficiency of the compressor in the heat pump process	$\eta_{HP,comp.}$	95	%
Temperature difference at the pinch point in the internal heat exchanger in the heat pump process	$\Delta T_{HP,iHX}$	5	K
Pressure loss of the internal heat exchanger in the heat pump process	$\Delta p_{HP,iHX}$	0	bar

Table 2. Reference parameters of the thermal storage.

Parameter	Abbreviation	Value	Unit
Efficiency of the thermal storage	η_{st}	100	%
Temperature difference when charging the thermal storage	$\Delta T_{st,in}$	10	K
Temperature difference when discharging the thermal storage	$\Delta T_{st,out}$	16.5	K
Minimum temperature of the thermal storage	$t_{st,min}$	90	°C
Maximum temperature of the thermal storage	$t_{st,max}$	120	°C
Temperature difference between thermal storage and HP/ORC at the pinch points	ΔT_{PP}	5	K

Table 3. Reference parameters of the ORC.

Parameter	Abbreviation	Value	Unit
Pressure loss at the evaporator in the ORC	$\Delta p_{ORC,evap.}$	0	bar
Pressure loss during condensation in the ORC	$\Delta p_{ORC,cond.}$	0	bar
Superheating temperature in the ORC	$\Delta T_{ORC,sh}$	0	K
Condensation temperature in the ORC	$t_{ORC,out}$	30	°C
Sub-cooling temperature in the ORC	$\Delta T_{ORC,sc}$	0	K
Isentropic efficiency of the ORC	$\eta_{s,ORC}$	70	%
Generator efficiency of the ORC	$\eta_{orc,gen.}$	95	%
Mechanical efficiency of the feed pump in the ORC	$\eta_{ORC,FP,mech.}$	80	%
Electrical efficiency of the feed pump in the ORC	$\eta_{ORC,FP,el.}$	95	%
Temperature difference at the pinch point of the internal heat exchanger in the ORC	$\Delta T_{ORC,iHX}$	5	K
Pressure loss of the internal heat exchanger in the ORC	$\Delta p_{ORC,iHX}$	0	bar

3. Results and Discussion

The results of the simulation work are presented in this section. Aspects such as the heat pump's COP and the ORC efficiency as a function of load are examined in more detail. The temperature profile of the storage is also mentioned and displayed depending on the load.

3.1. Key Performance Indicators of the Working Machines

At full load, the heat pump COP reaches up to 5.0 and the ORC has an efficiency of around 10.6%. This results in a P2P efficiency of approximately 52%. The P2P course as

a function of the load, which is set by the mass flow and the temperature drop after the thermal storage ΔT_{PL}, is shown in Figure 3. The mass flow was varied at intervals of 10% and the temperature drop in 5 K steps. Each node represents a separate operating point.
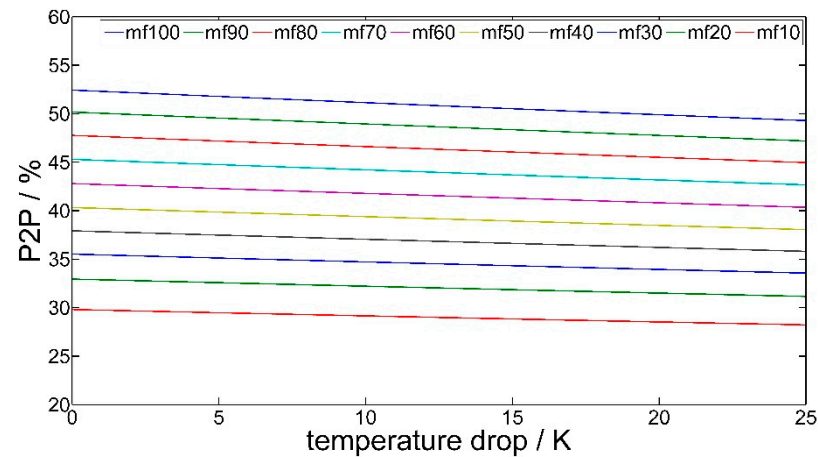

Figure 3. P2P as a function of mass flow (mf) and temperature drop after the thermal storage of the HP-ORC-system using R1233zd(E).

Figure 3 shows that the reduction in mass flow causes a large drop in P2P efficiency. The temperature change covers a relatively small range, considering that the maximum temperature drop shows a transition from 393.15 K to only 363.15 K. However, a temperature drop still has a noticeable effect on the isentropic efficiency. As was mentioned in Section 2.4.2, the drop in temperature affects the pressure level, which ultimately influences the isentropic efficiency through the volumetric efficiency in equation (9).

There is no correspondingly large difference when comparing the P2P value for full load operation (52%) with that of the part load case (about 40%) at a considerable temperature drop of 20 K, as well as a mass flow of 50%. This means that at half load, approximately one fifth of the P2P efficiency is lost. These results are in agreement with those of Liu et al. [26], who also practically showed that their application had realistic efficiencies. The results would be similar for other machines, since only properties such as the motor efficiency differ. Overall, a drop in the storage temperature does not cause such large losses of the P2P efficiency compared to reducing the mass flow.

3.2. Shifting of the Pinch Point

In addition to the key performance indicators, the shift of the pinch point is also examined more closely using *t*, *Q*-diagrams, which are shown in the following graphs. The pinch point analysis is explained in detail in the Appendix of reference [24].

Figure 4a shows the *t*, *Q*-curve for R1233zd for full load operation and for the part load case at a relative mass flow of 50% in both HP and ORC operation. The slight, horizontal shift of the pinch point for both operating cases shows the negative effect of the mass flow on the isentropic efficiency, which is explained as follows:

After the working medium has been brought to a higher temperature level by the compressor in HP operation, it then releases its heat to the thermal storage. Due to the poorer efficiency of the compressor at a mass flow of 50%, which leads to increased dissipation energy, the working medium has a higher temperature after compression and at the beginning of the heat transfer to the storage. Accordingly, the pinch point of the HP process is shifted horizontally by about 2.5 percentage points (ppt) compared to the full load case, because the higher inlet temperature of the superheated steam requires more cooling to reach the state of saturated steam.
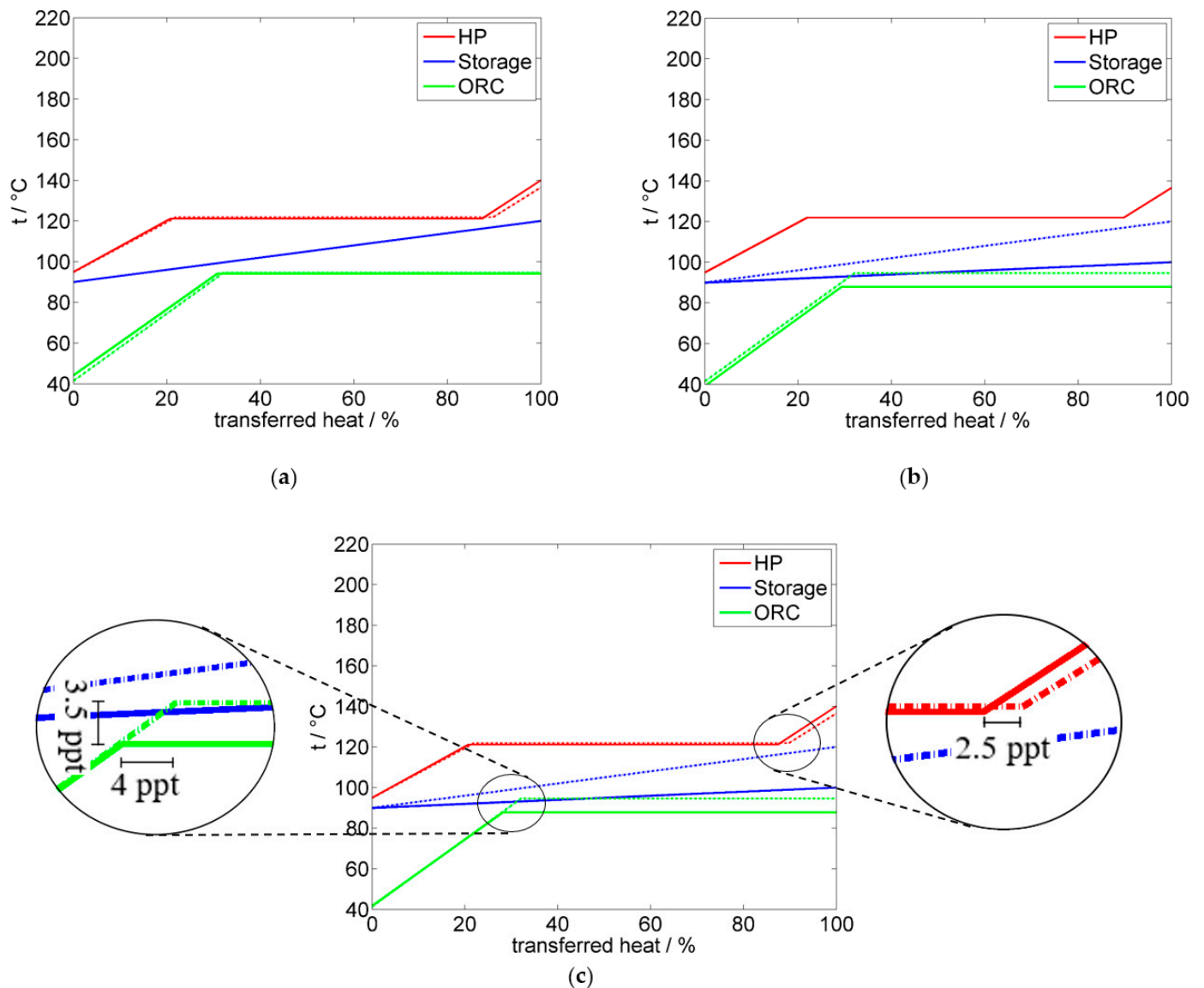
Figure 4. *t, Q*-diagram comparing the full load case (dashed) with the part load cases for 50% mass flow in (**a**), a 20 K temperature drop after the thermal storage in (**b**) and both effects combined as well as the pinch point shifts in (**c**).

In ORC mode, the working medium is evaporated while absorbing heat from the storage. The lower isentropic efficiency of the expansion machine is noticeable for the part load case with 50% mass flow, because the final temperature is about 5 K higher than in full load operation. Since the heat absorption from the storage takes place at a slightly lower pressure level, the pinch point for ORC operation is also slightly horizontally shifted to the left by about one ppt, so that a slightly increased heat transfer is required for condensation. This is because higher pressures are accompanied by higher evaporation temperatures.

The effects of a temperature drop in the thermal storage of 20 K for R1233zd is displayed in Figure 4b. The temperature difference in the storage is clearly recognizable by the decreased straight gradient of the storage temperature. Since the mass flow in this operating point is 100%, there is no horizontal shift of the pinch point for the HP process as is the case in Figure 4a. In fact, the process remains unchanged in this case.

For the ORC process, both a horizontal and a vertical shift of the pinch point can be observed. The horizontal displacement indicates that, as mentioned above, a larger amount of heat is required for evaporation. The vertical shift by about 7 K, which is more pronounced this time compared to the part load case at 50% mass flow, indicates that evaporation takes place at a significantly lower temperature level, since otherwise

there would be an overlap between the temperature curves of the ORC and the thermal storage. It is not possible for the medium to reach the same, let alone a higher temperature, compared to the full load case, at the exit of the thermal storage. Therefore, the temperature for the pinch point must drop.

Figure 4c shows that the characteristics of the individual part load variants overlap when they are combined. Consequently, the HP process behaves like the part load case with 50% mass flow (see case (a)). For the ORC, the pinch point undergoes an additional horizontal shift due to the changed mass flow. In this case, the combined effects cancel each other out when it comes to the expansion end temperature of the ORC, which results in identical inlet and outlet temperatures at the IHX (internal heat exchanger).

These results show that a decrease in the storage temperature leads to a minor negative effect for the P2P efficiency compared to the part load behavior through reduced mass flow. The loss of thermal energy is not entirely considered in this calculation, it directly affects the P2P efficiency of the system in two ways: On the one hand, the loss of the thermal energy, which cannot be converted back into electrical power, affects the P2P efficiency. On the other hand, the loss of thermal energy results in reduced temperatures (between 90 °C and 120 °C) of the thermal storage, which is considered a reduction in the maximum storage temperature and the temperature induced part load of the ORC. For a better understanding of both effects, a dynamic simulation of the state of charge and the different temperature layers in the thermal storage is currently in development to fill this gap. This includes strategies to handle the reduced temperature layer either via HP or ORC.

3.3. Implementation of the PTES in a Small Energy Grid

In this section, an implementation of the HP-ORC system in a small energy grid is studied based on the data of a dynamic load analysis and the previously developed model. For the simulation, the software AnyLogic [34] and the previously developed "i7-AnyEnergy" software library were used. The library contains modular components of energy systems, for example, PV or battery storages, which allows representation and simulation of complex smart grid applications. The simulation setup consists of a small settlement of 40 houses. Of these 40 houses, 20 are equipped with PV systems with a total installed capacity of 140 kW. For the power production of the PV system, solar irradiation data for the year 2016 from the German weather agency DWD [35] (Deutscher Wetterdienst) is used. The results of Tjaden et al. [36], in which electrical load profiles for residential buildings in Germany were created, are used to simulate the energy demand. The solar irradiance data for the city of Nuremberg in Southern Germany was considered. The maximum electrical power of the heat pump is 20 kW and up to 10 kW of electrical energy can be generated by the ORC. The thermal storage has a capacity of 1000 kWh thermal energy. This can be realized, for example, by a water storage with a volume of 28.6 m^3, which is equivalent to a tank of 2.5 m height and 1.9 m radius. For every minute of the year, the mentioned parameters were recorded and averaged over 24 h. Only the part load case due to changed mass flow was considered in this section.

As shown in Figure 5, the energy demand during the winter months is higher, but at the same time less electricity is supplied by the PV systems. This results in fewer ORC full load hours since the thermal storage is only charged when there is excess PV power to operate the heat pumps, which is rarely the case during winter.
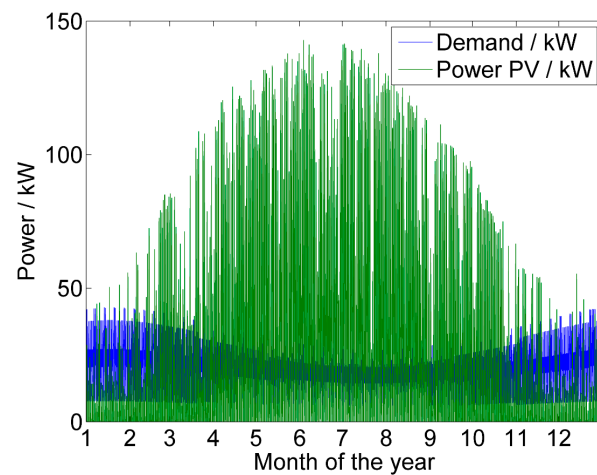
Figure 5. Course of the energy demand and energy supplied by the model PV system, based on irradiation data for Nuremberg, Germany in 2016.

Furthermore, Figures 6 and 7 show that the ORC operates more often under part load conditions during summertime, since the maximum ORC power output tends to be relatively low compared to the other seasons. The reason for this is a lower state of charge of the thermal storage during the winter season, therefore the ORC operates only for short periods of time with maximum output until the thermal storage is depleted. During summer, longer operation times with changing loads lead to a lower average power output from the ORC and therefore to a slightly lower ORC efficiency. On the other hand, the heat pumps operate at full load and the 1000 kWh capacity thermal storage is filled most of the time.

During the winter months, there are often periods when the ORC is not working. This is because the thermal energy storage is empty, as the PV energy can rarely cover the demand.
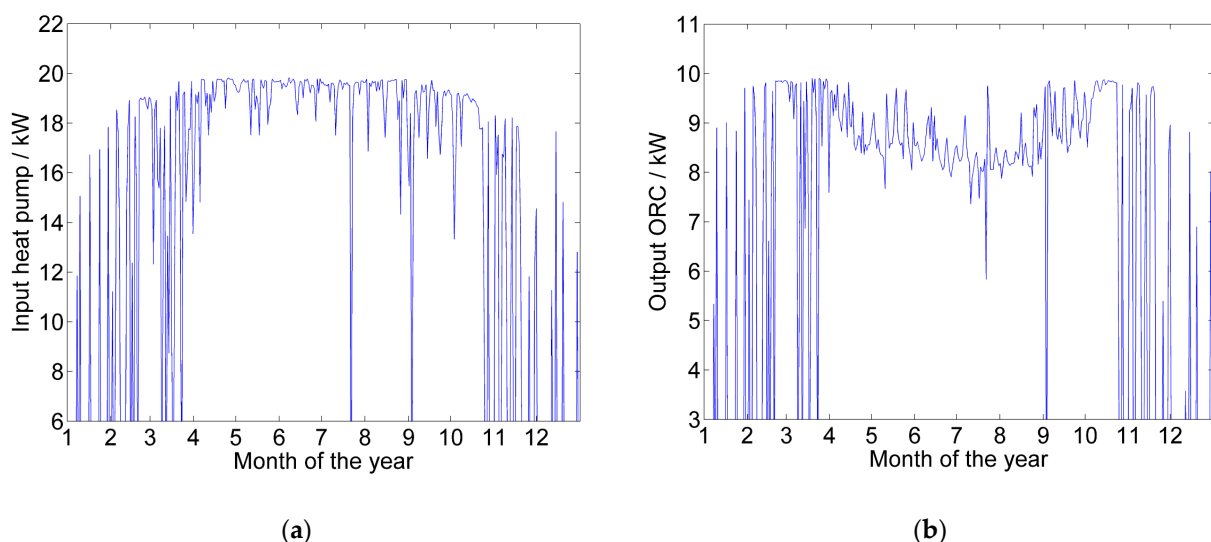

(**a**)

(**b**)

Figure 6. Average heat pump power input (**a**) and ORC power output (**b**) for the whole year of 2016.
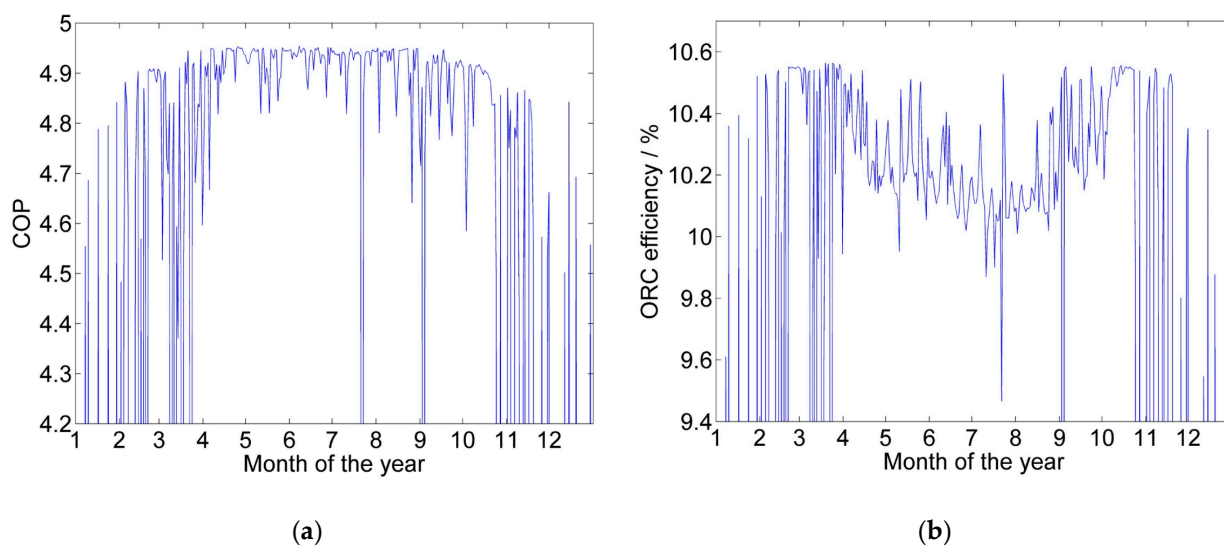
(**a**)   (**b**)

Figure 7. Average heat pump COP (**a**) and ORC efficiency (**b**) for the whole year of 2016.

Overall, there are 1979 full load hours (22.6% of the total time) for the heat pump and 1967 (22.5%) for the ORC throughout the year, where the average COP is 4.9 and the average ORC efficiency is 10.2%. The average heat pump load is 91.5% and the average ORC load is 88.5%. These values are collected in Table 4 at the end of this section. The loads refer only to times when the respective systems are in operation. The full load hours are not evenly distributed over the months.

Table 4. Overview of performance parameters for the investigated time frames.

Parameter	January	April	July	October	Year	Unit
Full load hours HP	13.5	261.6	249.5	154	1979	hour
Mean COP	4.8	4.9	4.9	4.9	4.9	-
Mean HP load	77.1	94.5	95.3	88.8	91.5	%
Full load hours ORC	7.5	263	247.2	157.7	1967	hour
Mean ORC efficiency	10.3	10.3	10.1	10.5	10.2	%
Mean ORC load	91.5	89.9	83.1	96.4	88.5	%
Maximum SOC	20	100	100	100	100	%

The months of July and January are examined in more detail below. While there is a lot of excess PV energy in July (see Figure 8), the thermal storage is rarely filled in January (see Figure 9). In fact, in January the energy supplied by PV is so low that the various demand peaks during the day are recognizable, which occur in the morning on workdays, at noon, and in the evening.
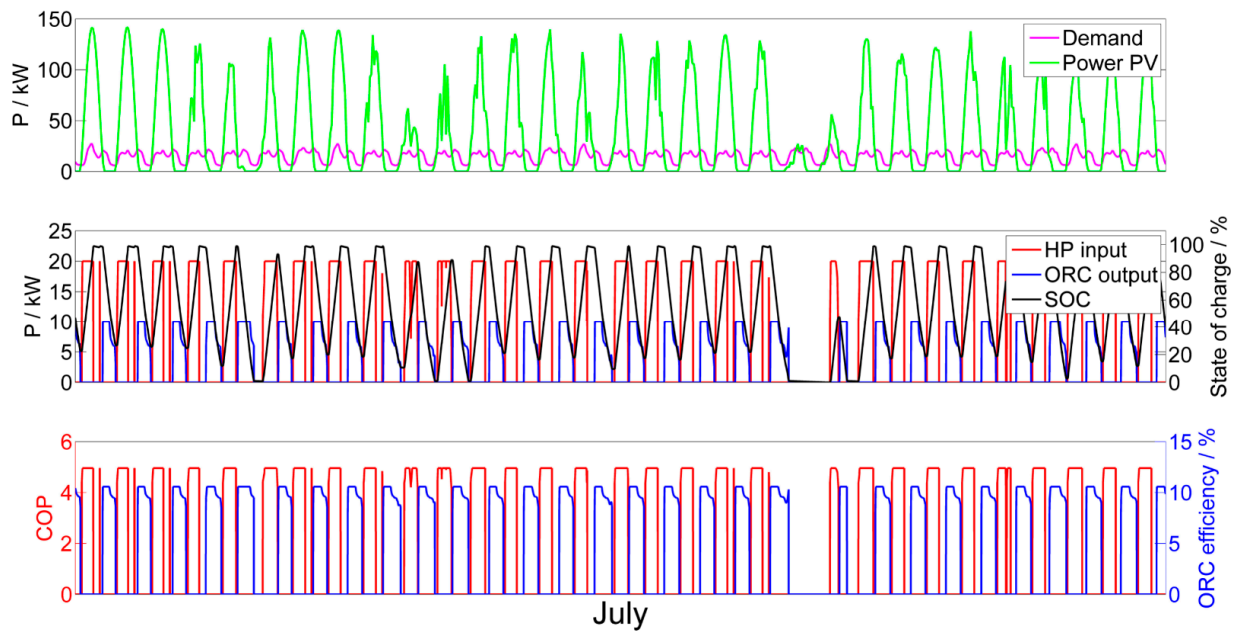
Figure 8. Course of the energy demand, energy input coming from the HP, state of charge (SOC) of the thermal energy storage, energy generated by the ORC, energy supplied by the PV as well as heat pump COP and ORC efficiency for July 2016.
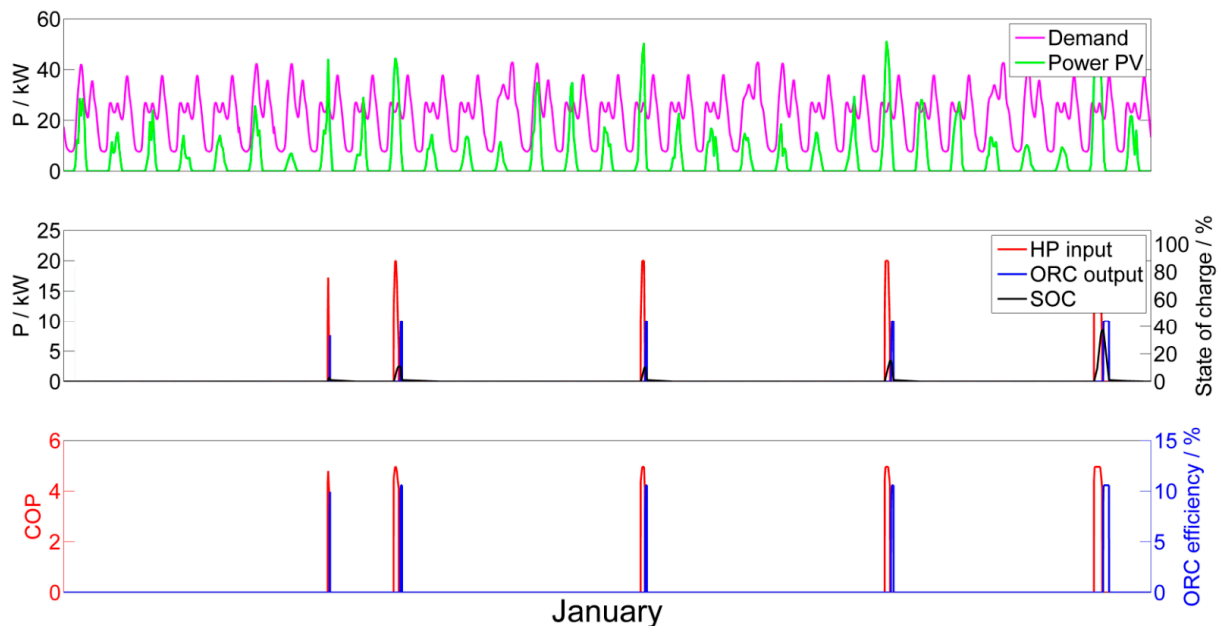

Figure 9. Course of the energy demand, energy input coming from the HP, state of charge (SOC) of the thermal energy storage, energy generated by the ORC, energy supplied by the PV as well as heat pump COP and ORC efficiency for January 2016.

In July, the heat pump operating time is equivalent to 249.5 full load hours, while its mean COP is 4.9. The average relative load is 95.3%. For the ORC, there are 247.2 full load hours and the mean ORC efficiency is 10.1% with an average relative load of 83.1% (see also Table 4). Most of the time, the state of charge (SOC) of the thermal energy storage reaches 100%. Moreover, it is shown that throughout the month of July the thermal storage is rarely completely discharged.

Gaps in the COP and ORC efficiency curves can be explained by the fact that on these days the PV energy does not exceed the demand, so that the thermal storage cannot be charged.

For January, the full load hours with 13.5 h for the heat pump and 7.5 h for the ORC turn out to be much smaller, as there are fewer opportunities to charge the storage due to the low PV energy. The average COP is 4.8 and the relative load is 77.1%. The average ORC efficiency is 10.3% with a load of 91.5%. Moreover, Figure 9 shows that the thermal storage gets charged and discharged only five times for the whole month of January, since those are the only times when the energy supplied by the PV exceeds the energy that is demanded. Most of the time, the thermal storage cannot even be charged to 20% of its maximum capacity. In July however, it is almost always fully charged.

Figures 10 and 11 show the PTES usage during the months of April and October. For April, the HP and ORC operating time are equivalent to 261.6 and 263 full load hours, which is more than July. Furthermore, a mean COP of 4.9 with a load of 94.5% and a mean ORC efficiency of 10.3 with a load of 89.9% also indicate that the whole system is closer to full load conditions compared to July. While the SOC reaches 100% several times, the storage is also completely discharged by the ORC.

In the month of October 2016, the HP and ORC operating times are only at 154 and 157.7 full load hours, respectively. This is because less energy is supplied from the PV systems during the last days of the month. Since the mean COP is at 4.9 with a load of 88.8% and the mean ORC efficiency is at 10.5% with a load of 96.4%, the PTES works close to full load conditions also in October. This indicates that, in terms of overall system efficiency, the PTES operates best in the months of fall and spring, when supplied and demanded energy are in better balance. However, during these seasons, there are more often shortages in supplied PV energy compared to summer.
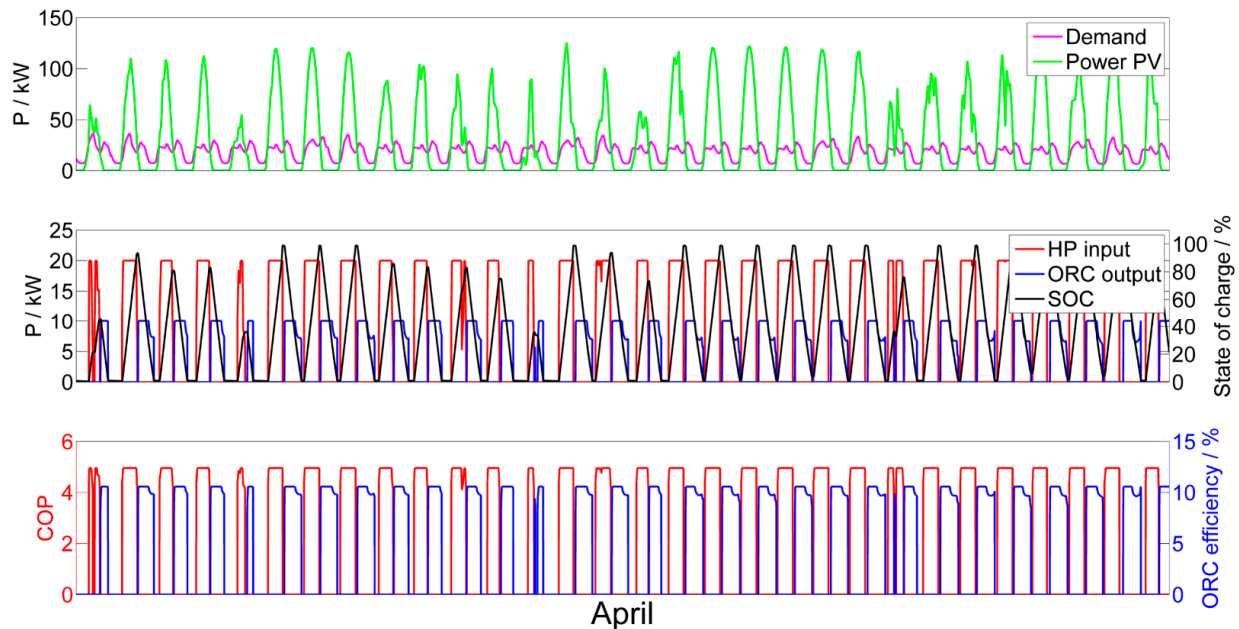

Figure 10. Course of the energy demand, energy input coming from the HP, state of charge (SOC) of the thermal energy storage, energy generated by the ORC, energy supplied by the PV as well as heat pump COP and ORC efficiency for April 2016.
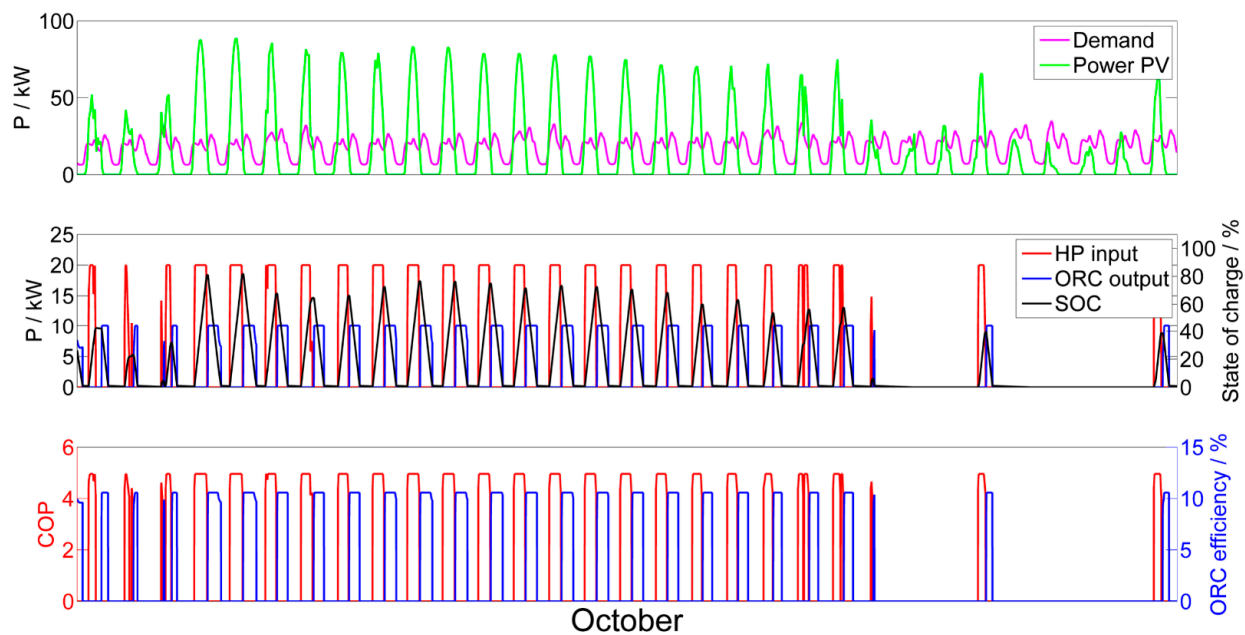
Figure 11. Course of the energy demand, energy input coming from the HP, state of charge (SOC) of the thermal energy storage, energy generated by the ORC, energy supplied by the PV as well as heat pump COP and ORC efficiency for October 2016.

4. Conclusions

In this paper, the part load behavior of PTES was investigated using modeling approaches. Part load of the HP-ORC system was adjusted by varying the mass flow and the temperature level of the thermal energy storage. As expected, all key performance indicators turned out to be lower compared to full load operation, because the HP-ORC system is no longer operated within a range that is optimal for the components used. Nevertheless, there is a possibility of keeping the efficiency as high as possible for the individual targeted performance range by a respective choice of working machines. Moreover, simulation results showed that there is no significant loss in P2P efficiency when comparing full load (52%) and part load operations (49%) for the mass flow.

In a theoretical implementation of the PTES on a small energy grid, data from the German weather agency DWD indicated that even under sub-optimal PV conditions, the used components of the PTES still run above 75% relative load.

In addition, the performance characteristics of PTES in relation to an annual PV course were examined in more detail. The challenge is that in the months of higher demand, such as November to February, the PV power is not sufficient to feed the HP-ORC system. However, the PTES worked almost continuously during the other months and is particularly reasonable during autumn and spring. In these seasons, the demand of electric energy is not too low, while the supplied PV energy is sufficient to charge the thermal energy storage.

It can be concluded that PTES may become important energy storage concepts in the coming years for bridging energy bottlenecks. However, PTES in combination with PV energy is especially reasonable for short-term or medium-term energy storage. Other approaches like chemical energy storage utilizing biomass, wind energy, or liquid organic hydrogen carriers (LOHC) are also required in order to realize a stable energy system.

Conflicts of Interest: The authors declare no conflict of interest.

Nomenclature

COP	Coefficient of Performance	-
FL	full load	-
HP	heat pump	-
ORC	Organic Rankine Cycle	-
P	power	W
P2P	Power-to-Power efficiency	%
PL	part load	-
PTES	Pumped Thermal Energy Storage	-
PV	photovoltaic	-
h	enthalpy	kJ/kg
Δp	pressure loss	Pa
p	pressure	Pa
ΔT	temperature difference	K
T	temperature	K
t	temperature	°C
Π	pressure ratio	-
α	load	%
κ	isentropic exponent	-
η	efficiency	%
Subscript		
comp	compressor	
cond	condenser	
el	electrical	
evap	evaporator	
exp	expander	
gen	generator	
IHX	internal heat exchanger	
m	motor	
mech	mechanical	
n	internal leakage	
pp	pinch point	
ppt	percentage point	
s	isentropic	
sc	super-cooled	
sh	super-heated	
st	storage	
v	volumetric	

Appendix A

This appendix provides calculated vapor pressures of the chosen working fluid using REFPROP, see Figure A1. The respective ORC working range of our setup is marked in red.
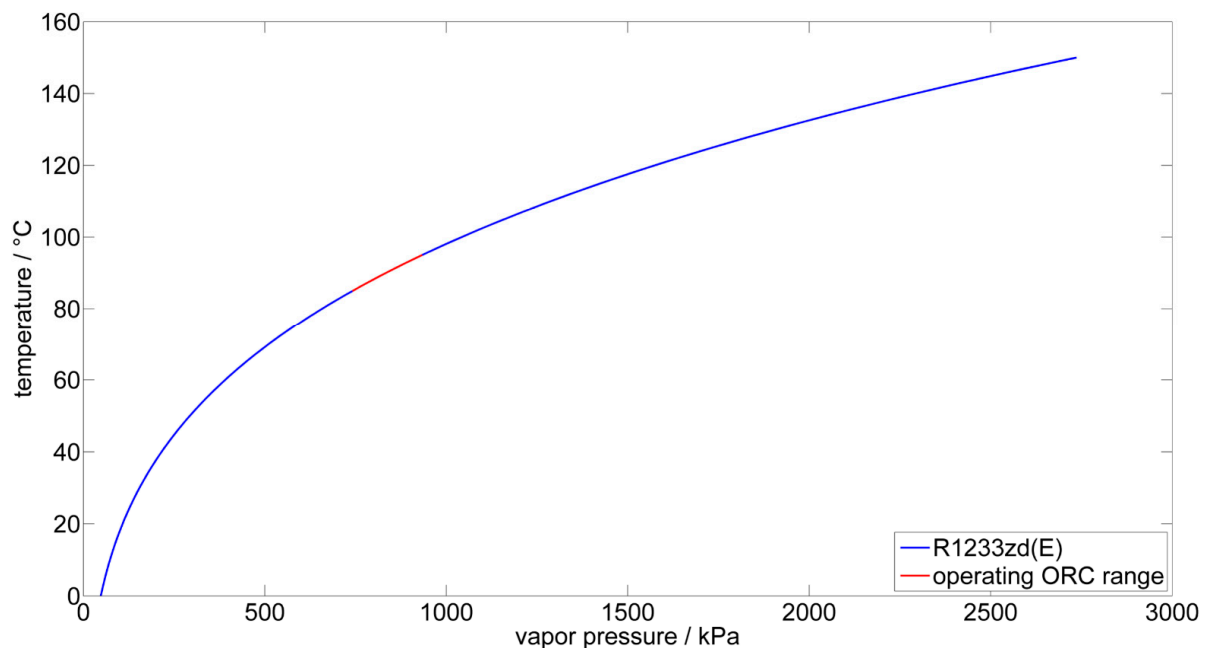
Figure A1. Vapor pressure curve for R1233zd(E) taken from REPFROP.

References

1. Inage, S. The role of large-scale energy storage under high shares of renewable energy. *Wiley Interdiscip. Rev. Energy Environ.* **2015**, *4*, 115–132. [CrossRef]
2. Dumont, O.; Frate, G.F.; Pillai, A.; Lecompte, S.; De Paepe, M.; Lemort, V. Carnot battery technology: A state-of-the-art review. *J. Energy Storage* **2020**, *32*, 101756. [CrossRef]
3. Frate, G.F.; Ferrari, L.; Desideri, U. Rankine Carnot Batteries with the Integration of Thermal Energy Sources: A Review. *Energies* **2020**, *13*, 4766. [CrossRef]
4. Mofijur, M.; Mahlia, T.M.I.; Silitonga, A.S.; Ong, H.C.; Silakhori, M.; Hasan, M.H.; Putra, N.; Rahman, M. Phase Change Materials (PCM) for Solar Energy Usages and Storage: An Overview. *Energies* **2019**, *12*, 3167. [CrossRef]
5. Köhler, T.; Kögl, T.; Müller, K. Study of the Crystallization and Melting Behavior of a Latent Heat Storage by Computed Tomography. *Chem. Ing. Tech.* **2018**, *90*, 366–371. [CrossRef]
6. Ali, S.; Deshmukh, S. An overview: Applications of thermal energy storage using phase change materials. *Mater. Today Proc.* **2020**, *26*, 1231–1237. [CrossRef]
7. Magro, F.D.; Arreola, M.J.; Romagnoli, A. Improving energy recovery efficiency by retrofitting a PCM-based technology to an ORC system operating under thermal power fluctuations. *Appl. Energy* **2017**, *208*, 972–985. [CrossRef]
8. McTigue, J.; White, A. A Comparison of Radial-flow and Axial-flow Packed Beds for Thermal Energy Storage. *Energy Procedia* **2017**, *105*, 4192–4197. [CrossRef]
9. Zhao, B.-C.; Cheng, M.-S.; Liu, C.; Dai, Z.-M. Cyclic thermal characterization of a molten-salt packed-bed thermal energy storage for concentrating solar power. *Appl. Energy* **2017**, *195*, 761–773. [CrossRef]
10. Barreneche, C.; Fernández, A.I.; Cabeza, L.F.; Cuypers, R. Thermophysical characterization and thermal cycling stability of two TCM: $CaCl_2$ and zeolite. *Appl. Energy* **2015**, *137*, 726–730. [CrossRef]
11. Rahman, A.; Smith, A.D.; Fumo, N. Performance modeling and parametric study of a stratified water thermal storage tank. *Appl. Therm. Eng.* **2016**, *100*, 668–679. [CrossRef]
12. Martinot, E. Grid Integration of Renewable Energy: Flexibility, Innovation, and Experience. *Annu. Rev. Environ. Resour.* **2016**, *41*, 223–251. [CrossRef]
13. Hodge, B.-M.; Martinez-Anido, C.B.; Wang, Q.; Chartan, E.; Florita, A.; Kiviluoma, J. The combined value of wind and solar power forecasting improvements and electricity storage. *Appl. Energy* **2018**, *214*, 1–15. [CrossRef]
14. Denholm, P.; Hand, M. Grid flexibility and storage required to achieve very high penetration of variable renewable electricity. *Energy Policy* **2011**, *39*, 1817–1830. [CrossRef]
15. Wu, Z.; Sha, L.; Yang, X.; Zhang, Y. Performance evaluation and working fluid selection of combined heat pump and power generation system (HP-PGs) using multi-objective optimization. *Energy Convers. Manag.* **2020**, *221*, 113164. [CrossRef]
16. Lecompte, S.; Huisseune, H.; Broek, M.V.D.; De Schampheleire, S.; De Paepe, M. Part load based thermo-economic optimization of the Organic Rankine Cycle (ORC) applied to a combined heat and power (CHP) system. *Appl. Energy* **2013**, *111*, 871–881. [CrossRef]
17. Mounier, V.; Mendoza, L.C.; Schiffmann, J. Thermo-economic optimization of an ORC driven heat pump based on small scale turbomachinery and comparison with absorption heat pumps. *Int. J. Refrig.* **2017**, *81*, 96–110. [CrossRef]

18. Koohi-Fayegh, S.; Rosen, M. A review of energy storage types, applications and recent developments. *J. Energy Storage* **2020**, *27*, 101047. [CrossRef]

19. Delgado, M.G.; Ramos, J.S.; Domínguez, S.; Álvarez; Ríos, J.A.T.; Cabeza, L.F. Building thermal storage technology: Compensating renewable energy fluctuations. *J. Energy Storage* **2020**, *27*, 101147. [CrossRef]

20. Lee, D.Y.; Seo, B.M.; Hong, S.H.; Choi, J.M.; Lee, K.H. Part load ratio characteristics and energy saving performance of standing column well geothermal heat pump system assisted with storage tank in an apartment. *Energy* **2019**, *174*, 1060–1078. [CrossRef]

21. Anderson, T.; Morrison, G. Effect of load pattern on solar-boosted heat pump water heater performance. *Sol. Energy* **2007**, *81*, 1386–1395. [CrossRef]

22. Wang, X.; Shu, G.; Tian, H.; Feng, W.; Liu, P.; Li, X. Effect factors of part-load performance for various Organic Rankine cycles using in engine waste heat recovery. *Energy Convers. Manag.* **2018**, *174*, 504–515. [CrossRef]

23. Ziviani, D.; Suman, A.; Lecompte, S.; De Paepe, M.; Broek, M.V.D.; Spina, P.; Pinelli, M.; Venturini, M.; Beyene, A. Comparison of a Single-screw and a Scroll Expander under Part-load Conditions for Low-grade Heat Recovery ORC Systems. *Energy Procedia* **2014**, *61*, 117–120. [CrossRef]

24. Eppinger, B.; Zigan, L.; Karl, J.; Will, S. Pumped thermal energy storage with heat pump-ORC-systems: Comparison of latent and sensible thermal storages for various fluids. *Appl. Energy* **2020**, *280*, 115940. [CrossRef]

25. Eppinger, B.; Zigan, L.; Will, S. Simlation of a pumped thermal energy storage based on a reversible HP-ORC-system. In Proceedings of the 5th international seminar on ORC Power Systems, Athens, Greece, 9–11 September 2019; pp. 9–11.

26. Liu, J.; Li, Q.; Wang, F.; Zhou, L. A new model of screw compressor for refrigeration system simulation. *Int. J. Refrig.* **2012**, *35*, 861–870. [CrossRef]

27. Wennemar, J. Dry Screw Compressor Performance and Application Range. In Proceedings of the 38th turbomachinery symposium, Houston, TX, USA, 14–17 September 2009; pp. 149–156.

28. Dumont, O.; Quoilin, S.; Lemort, V. Experimental investigation of a scroll unit used as a compressor and as an expander in a reversible Heat Pump/ORC unit. In Proceedings of the 2014 Purdue Conferences, West Lafayette, IN, USA, 14–17 July 2014.

29. Yamamoto, T.; Furuhata, T.; Arai, N.; Mori, K. Design and testing of the Organic Rankine Cycle. *Energy* **2001**, *26*, 239–251. [CrossRef]

30. He, W.; Wu, Y.; Peng, Y.; Zhang, Y.; Ma, C.; Ma, G. Influence of intake pressure on the performance of single screw expander working with compressed air. *Appl. Therm. Eng.* **2013**, *51*, 662–669. [CrossRef]

31. Erhart, T.; Eicker, U.; Infield, D. Part-load characteristics of Organic-Rankine-Cycles. In Proceedings of the 2nd European Conference on Poly-Generation, Tarragona, Spain, 1 March–1 April 2011.

32. Gonçalves, J.M.; Melo, C.; Hermes, C.J.L.; Barbosa, J.R., Jr. Experimental mapping of the thermodynamic losses in vapor compression refrigeration systems. *J. Braz. Soc. Mech. Sci. Eng.* **2011**, *33*, 159–165. [CrossRef]

33. Eppinger, B.; Steger, D.; Regensburger, C.; Karl, J.; Schlücker, E.; Will, S. Carnot battery: Simulation and design of a reversible heat pump-organic Rankine cycle pilot plant. *Appl. Energy* **2021**, *288*, 116650. [CrossRef]

34. Bazan, P. Hybrid Simulation of Smart Energy Systems. Ph.D. Thesis, Friedrich-Alexander-Universität Erlangen-Nürnberg (FAU), Erlangen, Germany, 2017.

35. Deutscher Wetterdienst DWD. Available online: https://www.dwd.de/EN/climate_environment/consultancy/solarenergy/solarenergy.html (accessed on 3 April 2019).

36. Tjaden, T.; Bergner, J.; Weniger, J.; Quaschning, V. *Representative Electrical Load Profiles of Residential Buildings in Germany with a Temporal Resolution of One Second*; ResearchGate: Berlin, Germany, 2015.